PCCP

Accepted Manuscript

ROYAL SOCIETY OF CHEMISTRY

www.rsc.org/pccp

Poly(Vinylidene Fluoride)/La$_{0.5}$Sr$_{0.5}$CoO$_{3-\delta}$ Composites: Influence of LSCO Particle Size on the Structure and Dielectric Properties

K. S. Deepa, P. Shaiju, M. T. Sebastian, E. Bhoje Gowd* and J. James*

Materials Science and Technology Division,
CSIR-National Institute for Interdisciplinary Science and Technology,
Trivandrum- 695 019, Kerala, India

For table of contents only
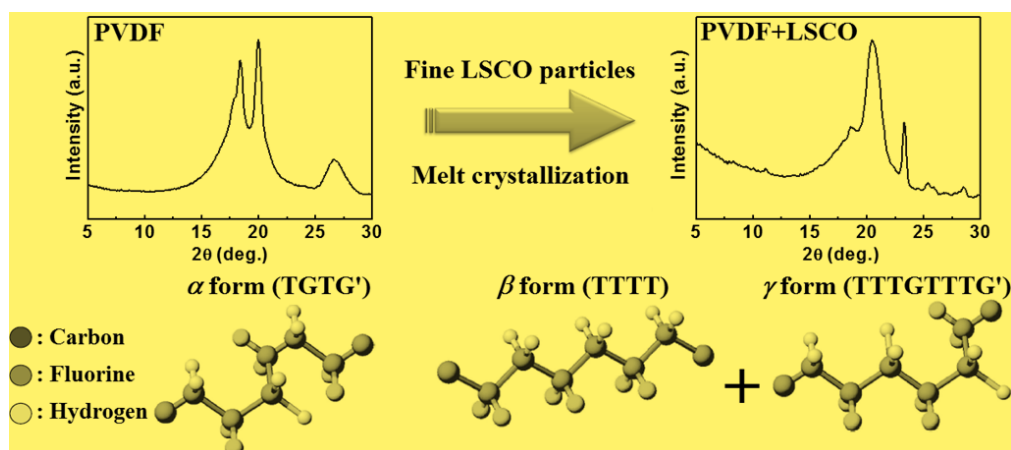
===
*Corresponding Authors:

E-mails: bhojegowd@niist.res.in and jamesj21058@yahoo.com

Tel: +91 471 2515474, +91 471 2515313, Fax: +91 471 2491712

1

Abstract

Dielectric composites composed of poly(vinylidene fluoride) (PVDF) and $La_{0.5}Sr_{0.5}CoO_{3-\delta}$ (LSCO) with high permittivity, low loss and high breakdown strength have been developed. The effects of particle size of LSCO (fine (~250 nm) and coarse (~3μm)) on the phase crystallization of PVDF and dielectric properties of polymer-LSCO composites are studied. The inclusion of fine LSCO into PVDF readily favours the formation of polar crystals (β and γ-phases), which makes the composite suitable for both electromechanical and high charge storage embedded capacitor applications. Moreover the addition of fine LSCO particles also increases the overall crystallization rate as well as the melting point of PVDF. Composite containing fine LSCO particles gave a percolation threshold at about 25 volume percentage, while those with coarse particles did not show any percolation even at very high volume percentage. As a result of fine LSCO particles loading, the composite exhibited relative permittivity (ε_r) value of ~600, conductivity of 2.7×10^{-7} S/cm, dielectric loss (tan δ) of 0.7 at 1 kHz and breakdown voltage of 100 V even at 20 volume percentage of filler, demonstrating promising applications in the embedded capacitor applications.

Keywords: Polymer-matrix composites, dielectric composites, Poly(vinylidene fluoride), $La_{0.5}Sr_{0.5}CoO_{3-\delta}$, ferroelectric

1. Introduction

Rapid growth in mixed-signal integrated circuits (ICs) has increased the need for multifunctional and miniaturized components in electronic applications. Discrete passives are the major barrier for the miniaturization of electronic systems as they outnumber the active ICs and occupy more than 70% area of the substrate.[1,2] Passive devices include resistors, capacitors, inductors etc. and among these more than 60% are capacitors. Also, the speed of ICs can be improved by using decoupling capacitors with higher capacitance and at shortest distances to improve switch performance. Here embedded decoupling capacitors are considered good alternatives, as they can provide a better electrical performance, higher reliability, lower cost, and improved design options.[1,2] Since embedded capacitors are restricted to limited area, a high capacitance, low dielectric loss, low leakage current, high breakdown voltage and adequate stability are the basic requirements for their real application.[3] Several approaches have been made to develop materials with high permittivity. Ferroelectric ceramics such as $BaTiO_3$, $BaSrTiO_3$, $PbMgNbO_3$-$PbZrTiO_3$ etc., were studied for this purpose.[4-6] Ceramic-metal composites were also investigated for enhancing the relative permittivity.[7-10] However, their relatively higher sintering temperatures limit their application due to the oxidation of metals. Recently, Anjana et al. reported that perovskite $La_{0.5}Sr_{0.5}CoO_{3-\delta}$ conducting ceramic can be used for enhancing the relative permittivity of CeO_2 ceramics, which avoids the oxidation problem of the metallic conductors.[11] Ceramic-polymer composites have been of great interest as embedded capacitor materials since they combine the processability of polymer with high relative permittivity of ceramics. Several studies have been done in ceramic-polymer composites adopting traditional ceramic phases like $BaTiO_3$, PZT,PMN-PT etc., as

3

filler.[12-14] Though a relatively higher permittivity and low dielectric loss is achieved in such composites, the required dielectric behaviour could be accomplished only at higher filler loading (>50 vol%) which further deteriorates the mechanical flexibility of the composites and the resulting printed wiring boards (PWBs). Polymer-metal composites were also studied as the metallic filler can provide improved dielectric behavior even at lower filler loading.[15-18] But the major drawback which limits their application is metals are liable to oxidation when the composite faces varying surrounding environment (eg. temperature, moisture etc.). This results in variation of the final properties of composites. Hence to overcome the difficulties associated with change in the properties of conducting phase due to oxidation problem of metals, Sumesh and Sebastian used conducting LSCO ceramic phases for preparing the insulator – conductor: polystyrene-$Ca[(Li_{1/3}Nb_{2/3})_{0.8}Ti_{0.2}]O_{3-\delta}$-LSCO composites.[19] In the present work, insulator – conductor composites comprising ferroelectric polymer PVDF and conducting LSCO ceramic phases were prepared.

A number of approaches such as, solid state calcinations, combustion synthesis, spray pyrolysis, sol-gel, co-precipitation, hydrothermal, etc. have been utilized to prepare LSCO powders.[20-22] Strontium substitution brings remarkable changes in the structural properties and gives a complex phase diagram to the LSCO system.[23,24] As the strontium content increases, LSCO exhibits a shift in crystal structure from rhombohedral to cubic (for x>0.4). Metallic behavior is observed for cubic LSCO, while the rhombohedral phase shows semiconducting behavior. The conductivity of cubic crystalline LSCO (> 1000 S/cm) is comparable to that of metals.[24-28] When x=0.5 ($La_{0.5}Sr_{0.5}CoO_{3-\delta}$) LSCO has conductivity of ~$1.1x10^4$ S/cm.[29]

The matrix chosen for the present study is a ferroelectric polymer (PVDF), which is known for its outstanding electroactive property, nonlinear optical susceptibility and high dielectric constant compared to other polymers. They also show good piezoelectric and pyroelectric responses, low acoustic impedance.[15] However, to increase the scope of their applications, it is highly necessary to improve the dielectric constant of PVDF. One simple method to increase the dielectric constant of PVDF is the introduction of ceramic particles with high dielectric constant into the polymer matrix.[30-34] However, it is difficult to obtain composites with very high dielectric constant (above 100) even with high filler content. Another method to improve the dielectric constant is the introduction of conducting fillers into the polymer matrix to achieve percolative composites.[35-39] A composite of LSCO with PVDF combines the positive aspects of ceramic as well as polymer. That is it combines the mechanical properties of polymer, conducting behavior of LSCO and also avoids the oxidation problem of metals on heat treatment at elevated temperatures and their composition can be widely tuned to get desired dielectric behavior.

In the present work, we first prepared the PVDF - LSCO composites with high permittivity and low dielectric loss. LSCO particles having different sizes are incorporated into PVDF by solution blending method and then hot pressed into pellets to study the properties of composites. It was found that fine LSCO, which dispersed homogeneously in the PVDF matrix have the ability to nucleate the polar crystals of PVDF and significantly modify the crystallization and melting behavior of PVDF. To the best of our knowledge, this is the first report to demonstrate the formation of polar crystals using LSCO particles. In second part of the work, the effects of LSCO characteristics on the properties of such conductor-insulator composites are discussed. It

5

was found that composite of PVDF- fine LSCO particles showed better dielectric and conducting behavior than PVDF with coarse LSCO composites.

2. Experimental

2.1. Samples preparation

$La_{0.5}Sr_{0.5}CoO_{3-\delta}$ samples were prepared as coarse grained powders by the solid state method and as fine particles by a precursor combustion method. Coarse grained samples of LSCO were prepared by conventional solid state reaction of a stoichiometric mixture of La_2O_3, $SrCO_3$ and Co_2O_3 at 1100^oC for six hours. To prepare fine particles of LSCO, analytical grade La_2O_3 (99.99% from Treibecher, Austria, Europe), $Co(NO_3)_2.6H_2O$ (99% from S. d. Fine-Chemicals Ltd, Mumbai), $Sr(NO_3)_2$ (99.5% from Central Drug House Ltd, Mumbai), Citric acid ($C_6H_8O_7.H_2O$) and ethylene glycol (99.5% from S. d. Fine-Chemicals Ltd, Mumbai) were used as starting materials. La_2O_3 was dissolved in nitric acid and salts of strontium and cobalt were dissolved in water. Solutions containing La^{3+}, Co^{2+} and Sr^{2+} ions were mixed in the ratio required for the formation of LSCO and to this solution, sufficient amounts of citric acid and ethylene glycol were added for complete complex formation. The pH of the solution was adjusted to nearly neutral by addition of ammonia solution. This solution was then heated slowly till excess water is evaporated to form a syrupy liquid, which subsequently gets converted to a transparent viscous gel. On further continuous heating the gel gets converted to dark blue foam, which finally gets auto-ignited giving a voluminous and fluffy product of combustion. The powder thus obtained, was further heated at 650, 700 and 750^oC for

6

four hours to get crystalline LSCO. PVDF used for the present study was obtained from Aldrich chemicals.

PVDF-LSCO composites were prepared by dissolving required amount of PVDF in dimethyl formamide (DMF) and different volume fractions of both coarse and fine LSCO powders were individually added to the PVDF solution. The suspension is ultrasonically mixed for 30 minutes and then magnetically stirred at 60°C for 15 minutes. During the process the excess DMF in the mixture gets evaporated leading to a highly viscous mixture of PVDF and LSCO, which is then dried at 100°C.The resultant mixture was then hot-pressed at 190°C (pressure $\sim$ 10Mpa) into cylindrical pellets of about 11 mm diameter and 2 mm thickness. Copper leads were connected to pellets of these composites on both sides using silver paste and used for further dielectric and conductivity measurements.

2.2. Characterization

X-ray diffraction measurements of LSCO powders were obtained by PANalytical X'pert PRO (Netherlands) diffractometer using Ni-filtered Cu-Kα radiation. These measurements were performed in reflection mode in the 2θ range of 10-75°. X-ray diffraction measurements of PVDF and composites were carried out on a XEUSS SAXS/WAXS system using a Genixmicro source from Xenocs operated at 50 kV and 0.6 mA. The Cu Kα radiation (λ = 1.54 Å) was collimated with a FOX2D mirror and two pairs of scatterless slits from Xenocs. The 2D-patterns were recorded on a Mar345 image plate and processed using Fit2D software. These measurements were made in the transmission mode. The infrared spectra were measured with a Perkin Elmer series FT-IR spectrometer-2 over the wavenumber range of 4000 – 400 cm^{-1}. The powder sample

was mixed with KBr and pressed in the form of pellets for FTIR measurements. The FTIR spectra were collected with 32 scans and a resolution of 2 cm^{-1}.

The crystallization and melting behavior of all samples were measured using a differential scanning calorimeter (Perkin Elmer Pyris 6 DSC). The melt crystallization temperature (T_{mc}) was measured for PVDF and PVDF/LSCO composites. In this case, sample was first heated from room temperature to 190 °C (above melting temperature of PVDF) at a rate of 20 °C/min, where it was held for 2 min to erase the thermal history of the sample, then cooled at a rate of 10 °C/min to room temperature to measure the T_{mc}. All the samples were reheated to 190 °C to measure the melting temperature. In another set of experiments, crystallization half-time was measured at isothermal crystallization temperature. The thermal program employed for the isothermal crystallization is depicted in Fig. S1. A sample was heated from room temperature to 190 °C (above melting temperature of PVDF) at a rate of 20 °C/min, where it was held for 2 min to erase the thermal history of the sample, then cooled rapidly at a rate of 100 °C/min to a desired crystallization temperature (T_c) i.e. 140 °C, and kept for 30 min for the isothermal crystallization. All the DSC experiments were conducted under nitrogen atmosphere.

Scanning electron micrographs were obtained using Jeol JSM-5600LV (Japan) scanning electron microscope, using gold coated samples. The dielectric data of these samples were obtained from complex impedance measurements made using Hioki 3532-50 LCR Hi Tester (Japan) at frequencies ranging from 100 Hz to 3 MHz at room temperature. The breakdown voltages of the samples were measured using Keithley 2410, 1100 V source meter.

8

3. Results and Discussion

The X-ray diffraction patterns of LSCO prepared by citrate gel method and calcined at different temperatures between 650 and 750°C for four hours are given in Fig. 1. The XRD patterns of samples calcined at 650°C and 700°C shows characteristic reflections of LSCO. In addition to these reflections, few extra peaks are observed. Basal and Wine reported the similar X-ray pattern for the LSCO particles calcined at 550°Cand assigned these reflections to the mixture of LSCO, Co_3O_4, and $SrCO_3$.[40] It is also observed that with increase in calcination temperature intensity of reflections corresponding to LSCO increases and finally at 750°C, the compound showed reflections characteristics of pure LSCO. All the peaks were indexed based on the JCPDS file No.48-0122 and the pattern corresponds to the rhombohedral phase of LSCO.[24,28]
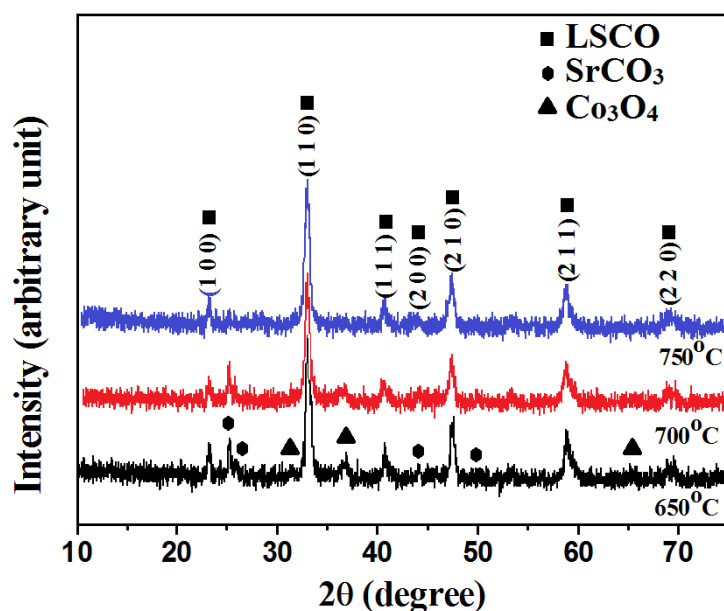
Fig. 1 XRD patterns of LSCO prepared by citrate gel method and calcined at different temperatures for 4 hours.

Fig. 2 shows the SEM micrographs of LSCO synthesized by solid state and citrate gel methods. The average grain size of LSCO particles measured from the micrographs was about 250 nm for fine and 3 μm for coarse particles of LSCO.
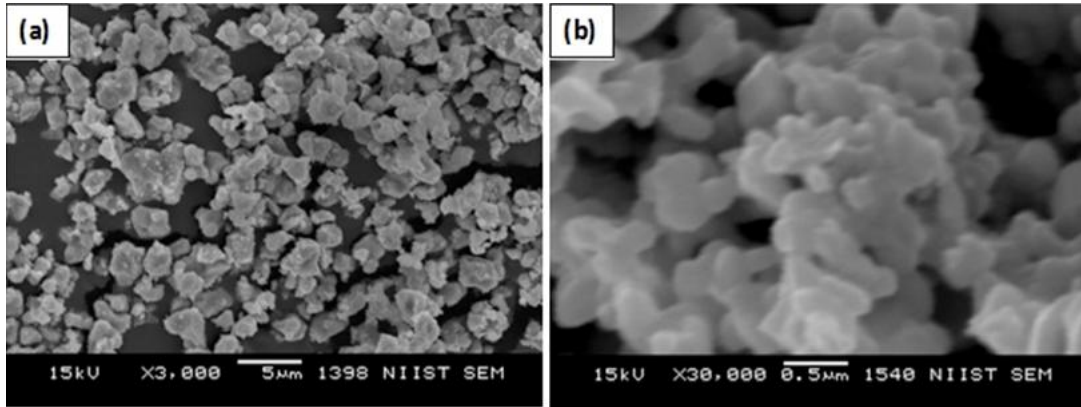
Fig. 2 SEM micrographs of LSCO prepared by (a) solid state method and (b) citrate gel method.

The SEM micrographs of the composites containing 20, 30 and 40 volume percentages of LSCO fine particles prepared by citrate gel method as well as 40 volume percentage of coarse LSCO obtained by conventional ceramic route are shown in Fig. 3. Uniform distribution of LSCO particles in the matrix can be clearly seen from the Figure. Though fine particles (Fig. 3(a-c)) have strong tendency for agglomeration, ultrasonic mixing and subsequent magnetic stirring at 60 ^{o}C made the filler particles to get uniformly dispersed in PVDF matrix. The surface morphology of composite with 40 volume percentage coarse LSCO (Fig. 3(d)) showed uniform distribution of filler particles in the matrix. However, these are large and well separated compared to composites (Fig. 3(c)) with same concentration of fine particles. This could explain the requirement of higher filler loading of coarse LSCO in PVDF to reach percolation than the composites with fine LSCO particles, which will be discussed in the next section.

10
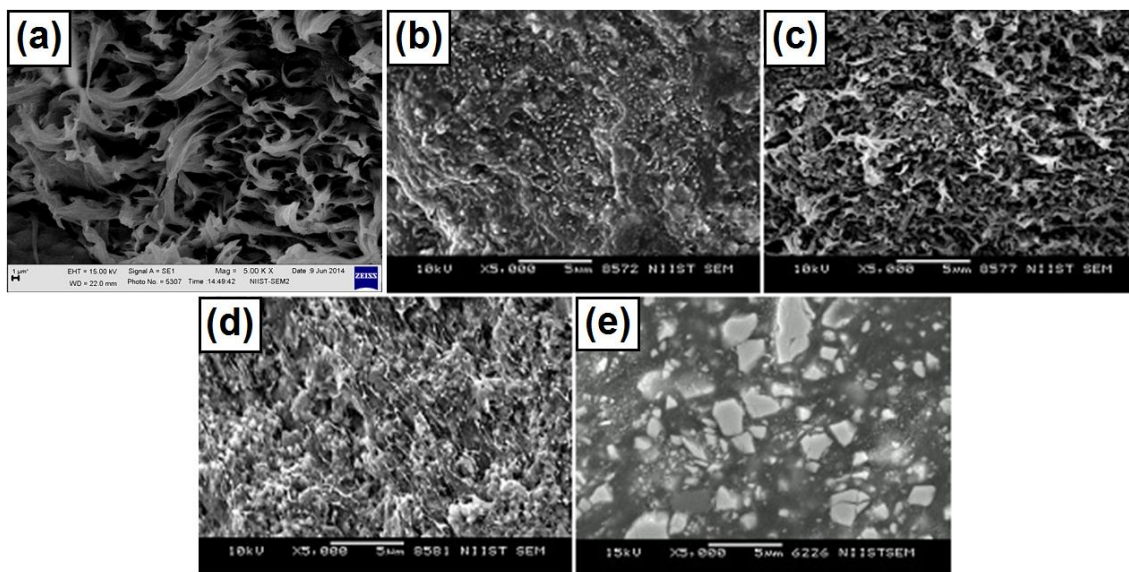
Fig. 3 SEM micrographs of (a) pure PVDF and PVDF/LSCO composites containing (b) 20, (c) 30, (d) 40 percentages of fine LSCO and (e) 40 percentage of coarse LSCO particles

Samples of PVDF/LSCO composites were fabricated through a simple solution blending and hot-pressing procedure and are directly used for further structural characterization. Before discussing the influence of LSCO on the crystallization behavior of PVDF, it is worth mentioning hereabout the crystalline phases of PVDF. PVDF exhibits very complex polymorphic behavior depending on the processing conditions and it appears in at least five crystalline forms i.e. α, β, γ, δ, and ε.[41-43] Compared to other crystalline phases, the polar β and γ phases have attracted much attention due to their unique properties and applications. PVDF in polar β and γ phases provides ferroelectric properties, such as dielectric properties and piezoelectric constant.[44-46] It is always a great challenge to obtain 100% polar crystals in PVDF by melt crystallization.
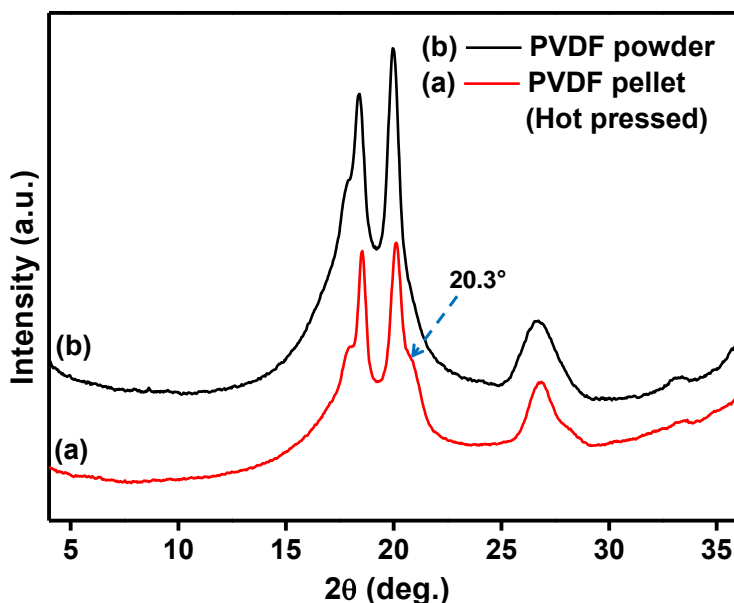
Fig. 4 Wide angle X- ray diffraction (WAXD) patterns obtained for (a) Hot pressed PVDF pellet and (b) PVDF powder.

The X-ray diffraction gives the direct information of the PVDF crystal forms. Fig. 4 shows the XRD patterns of PVDF powder and PVDF hot pressed pellet for the purpose of comparison. Powder sample shows characteristic reflections at 17.7^o, 18.4^o, 20.0^o, and 26.6^o which are assigned to (100), (020), (110), and (021) reflections of the α-phase.[47,48] For the pellet, all α characteristic peaks are still observed but with a tiny shoulder at around 20.3^o, the characteristic reflection of polar phases (β and/or γ).[49,50] It is already reported that the melt crystallization under high pressure and temperature can induce the formation of the β phase.[51,52] So the appearance of small fraction of β can be related with the experimental conditions used for the preparation of PVDF pellet.

12
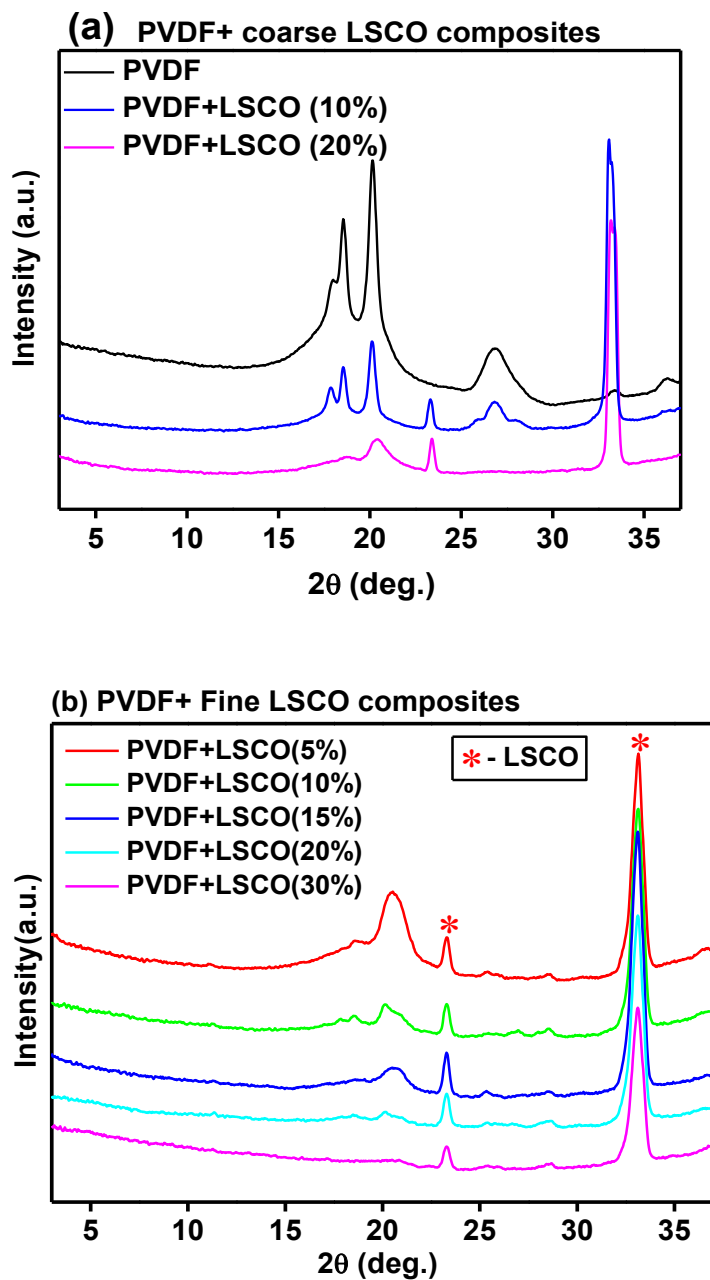
Fig. 5 WAXD patterns obtained for (a) PVDF/coarse LSCO and (b) PVDF/fine LSCO composites.

Fig. 5 shows the XRD patterns of PVDF/LSCO composites prepared with varying volume percentages of coarse and fine LSCO powders. All the reflections in the XRD patterns corresponded to either PVDF or LSCO.XRD patterns showed a decrease in the intensity of reflections corresponding to LSCO with its increasing volume percentages

due to the absorption of X-ray by LSCO particles. It is worth mentioning here that these XRD patterns are collected in the transmission mode. XRD patterns of PVDF/LSCO composites containing coarse grained LSCO show reflections characteristic of both α and polar phases (β and γ). The content of the polar phases increases with the increase in LSCO content. In contrast, no diffraction reflections of the α phase were seen in the XRD patterns of PVDF/LSCO composites containing fine LSCO, indicating the formation of pure polar phases.

The phase formation in PVDF with LSCO loading was also proved from the FTIR analysis. Fig. 6 shows the FTIR spectra of PVDF pellet and PVDF containing different volume percentages of fine LSCO particles. Strong absorptions bands at 532, 610, 762, 796, 978, and 1390 cm^{-1} are observed in FTIR spectra of the neat PVDF pellet indicates the formation of the non-polar α phase.[39,53] However, very weak peaks at 840, 1232, and 1275 cm^{-1} are also observed, which means that trace amount of polar crystals are also present in the PVDF pellet. In case of the composites with fine LSCO powder, no α phase bands were seen and only the bands for polar crystals are observed at 510 cm^{-1} for both β and γ phases, 1232 cm^{-1} for γ phase, 840 and 1275 cm^{-1} for β phase.[39,54,55] The FTIR results are in good agreement with X-ray diffraction results discussed in the preceding section. Since the FITR measurements were made in the transmission mode, there is a possibility for the radiation to get absorbed by LSCO. This made it difficult to observe the change in the fraction of polar crystals with the addition of LSCO.

14
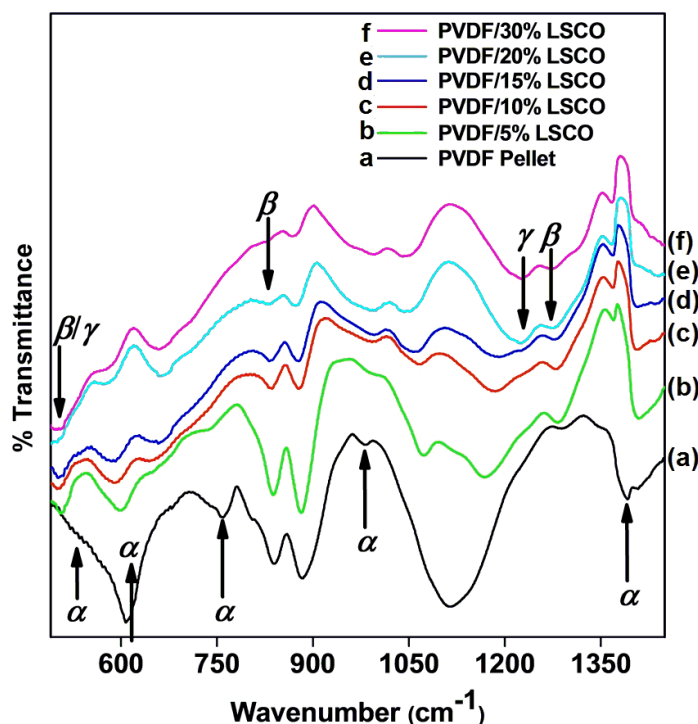
Fig. 6 Comparison of FTIR spectra obtained for pure PVDF and PVDF/fine LSCO composites.

Melting and crystallization behavior of PVDF and its composites were investigated by differential scanning calorimeter (DSC). Fig. 7a shows the DSC cooling thermograms of PVDF and its composites containing different volume percentages of fine LSCO particles at the cooling rate of 10°C/min. The melt crystallization temperature (T_{mc}) of pristine PVDF is 123°C. Incorporation of fine LSCO particles significantly shifted T_{mc} of PVDF to higher temperature around $141\text{-}143^{o}$C. The increase of T_{mc} indicates the enhancement of crystallization rate of PVDF in presence of fine LSCO particles. In order to further verify the crystallization rate of PVDF and its composites, crystallization half-time ($T_{1/2}$) was measured at an isothermal crystallization temperature at $140°$C. Fig. S1 shows the thermal program used for the isothermal crystallization of various samples.

15
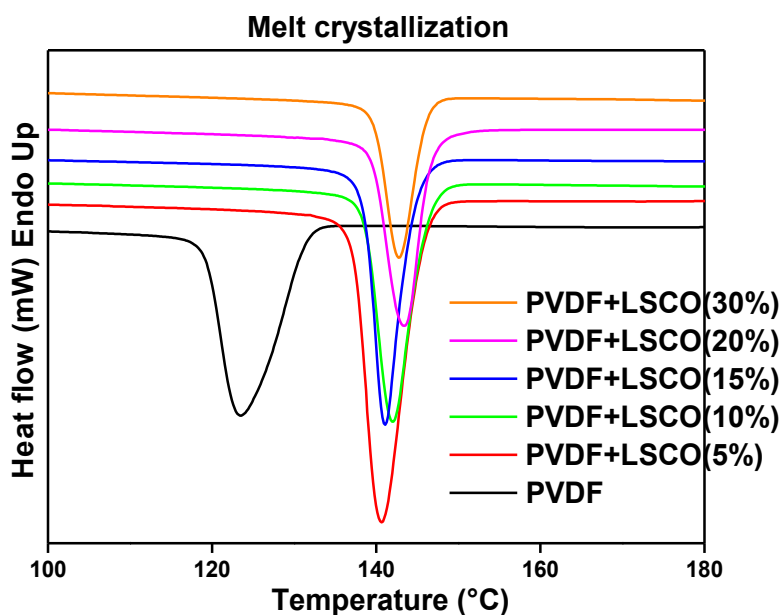
Fig. 7 Melt crystallization thermograms of PVDF and PVDF/fine LSCO composites.

The isothermal DSC thermograms of pure PVDF and its composites containing different volume percentages of fine LSCO are shown in Figs. S2 and S3. LSCO content dependence on $T_{1/2}$ of PVDF and its composites are shown in Fig. S4. $T_{1/2}$ measured for PVDF at 140°C is 400 s and it decreased dramatically to less than 40 s for fine LSCO containing PVDF composites. This means that the nano-sized LSCO particles act as nucleating agents, which have heterogeneous nucleation effect on accelerating the crystallization rate of PVDF. Such effects are consistent with other reports using different kinds of nanofillers.[56,57]

Fig. 8 illustrates the DSC second heating thermograms of PVDF and its composites using different volume percentages of fine LSCO. PVDF exhibits a broad melting peak at about 157°C. Such melting behavior arises due to melt recrystallization of α phase crystals.[58,59] After the addition of different volume percentages of fine LSCO, melting point of PVDF increases dramatically to 171°C irrespective of the volume

16

percentage of fine LSCO. DSC thermograms of PVDF-LSCO composites also show single sharp melting peak. This is most likely due to the heterogeneous nucleation induced by the LSCO particles, which promotes the formation of more uniform lamellae, that all melt at the same time during a heating cycle. It has been reported that the polar β and γ phases possesses higher melting temperature than that of the α phase.[56,60] These results clearly demonstrated that the addition of LSCO readily favours the formation of polar β and γ phases. These results are very much consistent with the XRD and FTIR data discussed in the preceding sessions.
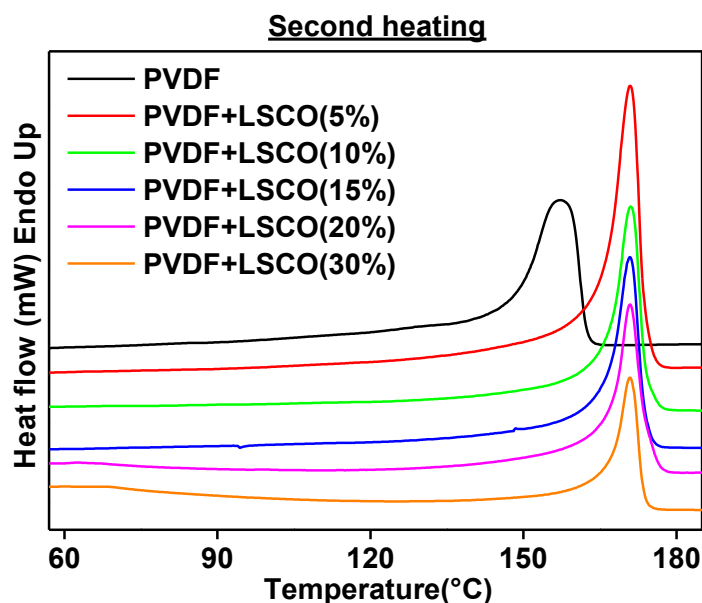
Fig. 8 DSC heating curves of PVDF and PVDF/Fine LSCO composites obtained from the subsequent heating of melt crystallized samples.

We also investigated the influence of coarse LSCO particles on the crystallization and melting behavior of PVDF. For that purpose, DSC thermograms were collected for the PVDF/LSCO composites containing 10 and 20 volume percentage of coarse LSCO powders. Fig. S5 shows the cooling DSC thermograms of

17

PVDF and its composites containing coarse LSCO particles. It is apparent from Fig. S5 that the coarse LSCO particles were also found to increase the T_{mc} of PVDF similar to the fine LSCO particles as discussed in the preceding section. Fig. S6 illustrates the second heating DSC thermograms of PVDF and its composites containing coarse LSCO particles. The melting temperature of the coarse LSCO containing composites is around $168^{o}C$, which is less than the T_m of fine LSCO containing composites ($171^{o}C$) and higher than T_m of PVDF ($157^{o}C$). These results suggest that PVDF composites containing coarse LSCO particles have both non-polar α and polar (β and γ) crystals, in agreement with the results of XRD as discussed in the preceding section.

XRD, FTIR and DSC results revealed that the presence of LSCO particles accelerate the crystallization rate of PVDF and induces the polar crystalline forms (β and γ). Lanceros-Mendez and co-workers demonstrated that the size of the nanoparticles determine the β content using nanometer size ferrite particles.[61] They also reported that the interaction between nanoparticles and PVDF chains induce all-trans conformation in PVDF segments, and then the structure propagates in crystal growth to generate β phase. It is also worth mentioning here that 100% polar phase formation by melt crystallization is always a challenge and recently Xing et al. achieved the formation of 100% polar crystals using ionic liquid modified carbon nanotubes.[39] They have shown that ionic liquid not only helps in homogenous dispersion of the carbon nanotubes in PVDF but also helps in PVDF chains to adopt the all-trans conformation to generate the polar crystals. Based on the literature[61] and the current study, we speculate here that the size of the particles and their homogenous distribution in PVDF matrix plays an important role in determining the content of the polar crystals of PVDF. In order to

18

further elucidate the mechanism of polar crystal formation in PVDF in presence of LSCO particles, a systematic study using low content of LSCO particles is necessary.

The variation of relative permittivity (ε_r), conductivity (σ) and loss tangent (tan δ) of the composites with different volume fraction of both coarse and fine LSCO particles, at 1 KHz are shown in Fig. 9. A gradual increase in permittivity and conductivity is observed for the composites containing both coarse and fine particles of LSCO. It can also be observed from the figure that a sudden increase in permittivity and conductivity occurs for composite with 25 volume percentage of fine LSCO particles. Whereas the composite containing coarse LSCO showed a steady increase even up to 60 volume percentage. 25 volume percentage gives the percolation threshold for PVDF- fine LSCO composites while the percolative behavior is absent even up to 60 volume percentage in the case of PVDF- coarse LSCO composites. This increase in dielectric behavior of the composites below percolation threshold is attributed to (i) polarization caused by the movement and entrapment of charge carriers at the interface creating a field leading to interfacial polarization[62] and (ii) the spatial distribution of LSCO particles in PVDF matrix, where filler particles in close proximity but blocked by thin barriers of dielectric material, form a large number of Internal Boundary Layer Capacitor (IBLC) structures[63] connected in series and parallel. The effective capacitance of all these capacitors in turn increases the overall dielectric behavior of the composites. When LSCO particles are introduced into PVDF matrix, it disturbs the force among the molecules of PVDF and thereby creates an interface with the matrix. Interface is the region around each LSCO particle where the intensity of any chosen property changes from LSCO to that of PVDF. In insulator-conductor composites the interfacial region is decided by the entrapped charge carriers at boundaries between two phases. The accumulated charge

19

carriers create an internal field which polarizes the surrounding matrix region forming a diffused double layer charge clouds.[64,65] At lower volume fraction due to randomly and well separated filler distribution, the interaction between the neighbouring particles will be negligible. With increase in LSCO content, number of particles per unit volume and its interfacial area with PVDF increases. This further enhances the average polarization associated with the particles and subsequently provides greater contribution to the permittivity of composite. Similarly in case of conductivity of composites at lower filler concentration due to higher interparticle distance, the energy level difference between the adjacent LSCO particles will be large and hence the electronic wave functions are localized within the grains of LSCO.[66] With increase in filler concentration the distance between some of the neighbouring particles get reduced in such a way that the energy difference will be less due to the overlapping of their double layer. This could delocalize the electron waves and further promotes tunnelling of electrons between the nearest neighbouring particles of LSCO.[67] This in turn increases the conductivity of the composite. With increase in filler concentration the probability of electron hopping increases and at percolation threshold the particles get arranged in such way that it can form random tunnelling network that spans the entire cross section of the composite giving rise to a sudden hike in conductivity of the composite.[68] Similarly, the resultant multipolar interaction of higher order between all neighbouring particles can account for the rapid increase in the permittivity of composites at percolation threshold.[69]

It is also clear from the Fig. 9(a) that variation in ε_r and σ of the composites with increasing filler content is much larger when fine particles of LSCO are used compared to coarse LSCO particles. This is because finer particles create large interface with the polymer imparting higher polarization to the composite resulting in superior property.

The values of permittivity, conductivity and loss tangent increase with the volume fraction of LSCO in the composites. At 20 volume percentage the composite could achieve optimum values of $\sim$ 600, 2.7×10^{-7} S/cm and 0.7 for ε_r, σ and tan δ, respectively.
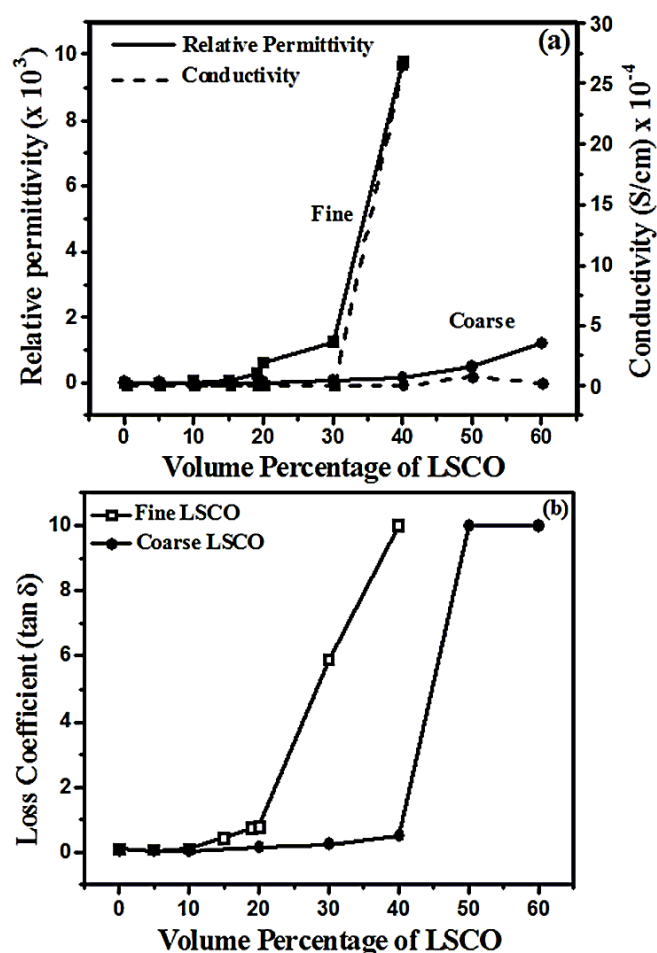
Fig. 9 Variation of (a) Relative permittivity and Conductivity (b) Loss tangent of PVDF composites with different volume percentage of LSCO at 1 KHz.

Since 20 volume percentage is well below the percolation threshold, the probability of breakdown of the composite due to percolation is very low. Thus this composite would be more suitable for applications in embedded passive devices. A similar relative permittivity of $\sim$ 500 could be achieved only at 50 volume percentage in

the composite containing coarse LSCO particles. Here due to higher filler concentration, the particles get dispersed in PVDF in such a way that a continuous conducting path could be easily formed. The effect is obvious from the high conductivity (5×10^{-5} S/cm) and tan δ (> 9) values (Fig. 9(a-b)) resulting from conduction loss due to dense packing. Such higher filler loading can also lead to loss of mechanical strength of these composites.

The variation of breakdown voltage with filler addition in both composites shown in Fig. 10 also confirms above discussion. The breakdown voltage is found to decrease with increase in filler concentration. The breakdown voltage for nanocomposites with 20 volume percentage of fine LSCO was 100 V and this decreased to below 10 V at 40 volume percentage (above the percolation limit). Similar behavior is noticed for coarse LSCO filled PVDF composites but the breakdown voltage was higher. The variation in dielectric and breakdown behavior of the composites could be explained based on the distribution of filler and polarization of matrix around each filler particle. Under applied field, the entrapped charge carriers at the interface create an internal field which in turn polarizes the surrounding matrix forming diffused double layer.[70] The extent up to which the field can polarize the matrix determines thickness of the double layer/tunnelling range.[71] With increase in volume fraction, number of particles increases and the inter particle distance decreases. At percolation the inter particle distance get reduced in such a way that the double layer around the nearest neighbouring particles overlaps leading to multipole coupling among the grains of LSCO and lower voltage is sufficient to cause breakdown.[72] At a given volume fraction, fine particles have higher filler density, higher surface area and lower inter particle distance compared to coarse LSCO particles in the composite. Therefore the rate of

22

decrease is higher for composites containing fine particles than those having coarse

LSCO particles.
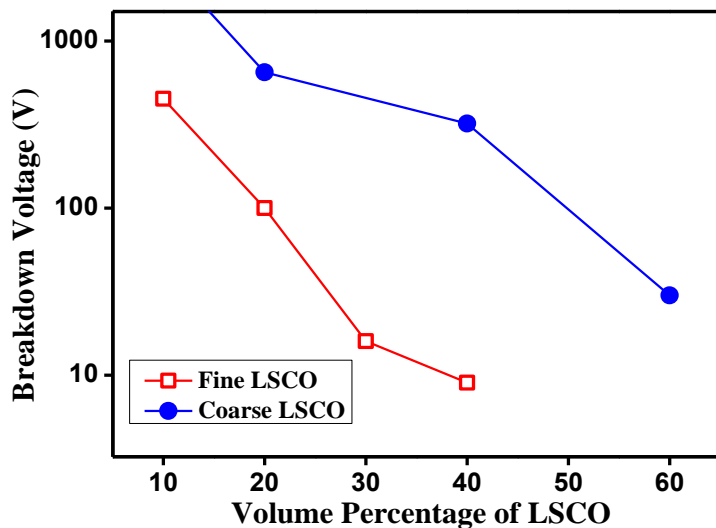
Fig. 10 Variation in breakdown voltage of PVDF-LSCO composites with different

volume percentages of both coarse and fine grains of LSCO.

Fig. 11(a-c) shows the variation in relative permittivity, conductivity and loss

tangent of PVDF- fine LSCO composites with frequency at different volume fractions

of filler. It is observed that up to 20 volume percentage of LSCO the composites

showed a gradual decrease in permittivity and loss tangent, while the conductivity

steadily increased with increase in frequency. It is obvious that above 20 volume

percentage ε_r, σ and tan δ remained constant (plateau region) at lower frequencies and

showed a linear dispersion at higher frequencies.
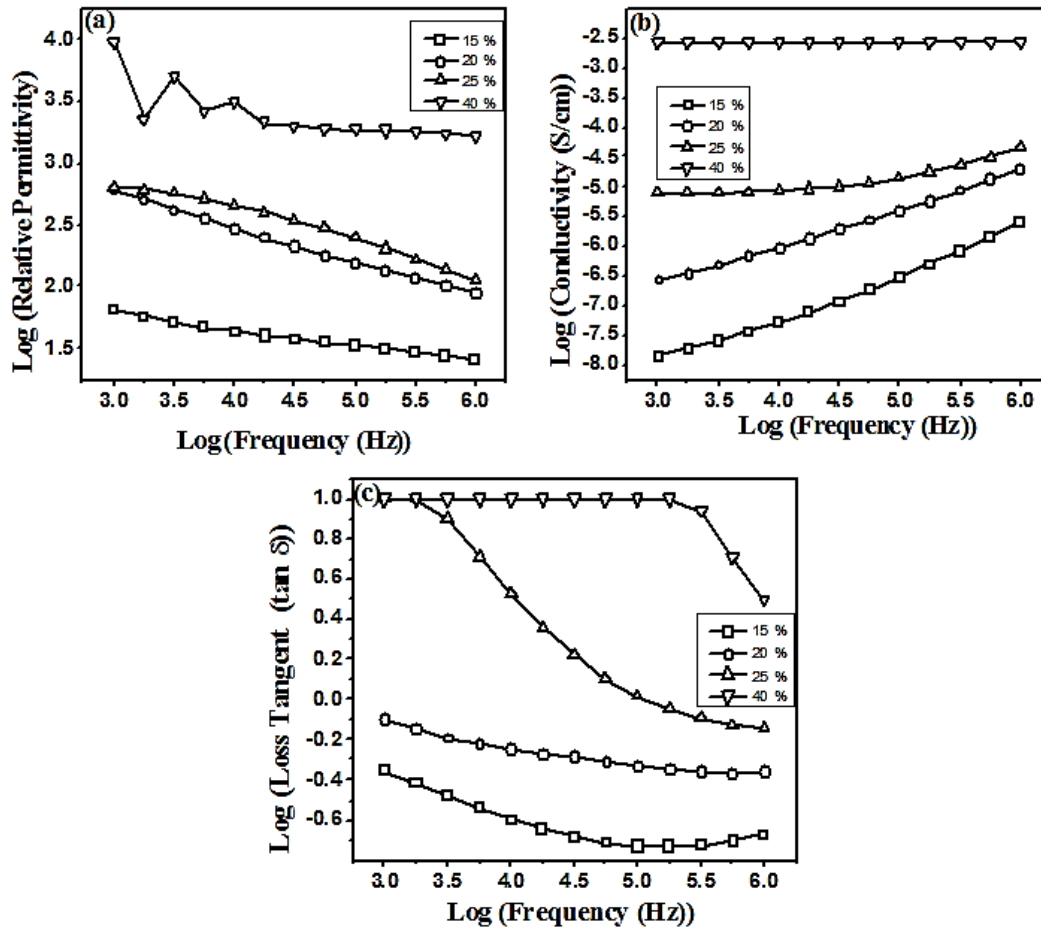
Fig. 11 Frequency dependence of (a) relative permittivity (b) conductivity and (c) loss tangent of PVDF- fine LSCO composites loaded with different volume percentages (15, 20, 25, 40).

In insulator- conductor composites conduction can occur by transfer of electrons between conducting particles in contact or through tunnelling of electrons between the nearest neighbours.[73] The dominating conducting mechanism in such composites is determined by the concentration and distribution of filler in the matrix. The strong frequency dispersion of conductivity (Fig. 11(a-b)) up to around 20 volume percentage of LSCO can be attributed to enhanced tunnelling current of the fine particle composites due to decrease in inter particle distance with increase in filler loading. The trend also indicate that percolation has not occurred up to this composition because

24

percolation is flow of charge through the conducting network that spans the entire cross section of the sample giving rise to frequency independent conducting behavior.[71,74] Therefore under applied field though the current increases by the movement of charge carriers, their entrapment at the interface highly localize the field and hence no charge flow occurs between the grains of LSCO. The phenomenon is also confirmed from the variation in the loss tangent with frequency (Fig. 11(c)). The tan δ value of the composite up to 20 volume percentage of LSCO is not more than 0.8 and decreased with increase in frequency. As can be seen from the fig. 11, when the filler concentration is above 20 volume percentage, the composite showed a steady and high value in the permittivity and conductivity at low frequency indicating that the inter particle distance of some of the randomly distributed particles get reduced in such a way to promote tunnelling of electrons between the grains of LSCO. The effect is confirmed by the higher value of loss tangent at low frequencies. With increase in filler loading the probability of electron tunnelling increases and so the frequency of transition from low frequency plateau to the dispersion region also increases. At 40 volume percentage the filler concentration increased in such a way that it can form a random network that spans the entire cross section giving rise to frequency independent conducting behaviour.

4. Conclusion

In summary, we have prepared dielectric composites using both fine (~250 nm) and coarse (~3μm) LSCO particles as fillers and PVDF as polymer matrix. Compared with the PVDF/coarse LSCO composites, polar crystals (β and γ- phases) are readily formed in the PVDF/fine LSCO nanocomposites. DSC study shows that fine LSCO has more efficient nucleating effects for PVDF crystallization and significantly increases the

melting temperature of PVDF to 171 $^{\circ}$C from 157 $^{\circ}$C. Composite of PVDF- fine LSCO particles showed better dielectric and conducting behavior than PVDF with coarse LSCO composites. Composite of PVDF with 20 volume percentage fine LSCO showed the property of high relative permittivity of $\sim$ 600 and relatively low conductivity and loss tangent of 2.7×10^{-7} S/cm and 0.7 respectively. Whereas in the composite filled with coarse LSCO particles, the similar property could be achieved only at 50 volume percentage which not only degrade the mechanical flexibility of the composite but also increases the dielectric loss leading to electrical breakdown even at lower voltage. Higher dielectric permittivity together with lower loss tangent and conductivity makes PVDF/LSCO nanocomposites as the suitable candidate for embedded capacitor application.

Associated Content:

Supporting Information Available: Fig. S1: DSC temperature programme used for the isothermal crystallization of PVDF and its composites. Fig. S2: DSC isothermal crystallization thermogram of PVDF at 140°C. Fig. S3: DSC isothermal crystallization thermograms of PVDF/fine LSCO composites at 140°C. Fig. S4: Variation in the

crystallization half time ($T_{\frac{1}{2}}$) with the increasing volume percentage of fine LSCO. Fig.

S5: DSC cooling curves obtained for PVDF and PVDF/Coarse LSCO composites. Fig.

S6: Variation in the melting point(T_m) of PVDF in the presence of coarse LSCO,

obtained from the second heating in DSC.

References

1   Y. Rao, S. Ogitani, P. Kohl and C. P. Wong, *J. Appl. Polym. Sci*., 2002, **83**, 1084-1090.

2   M. Kakimoto, A. Takahashi, T. Tsurumi, J. Hao, L. Li, R. Kikuchi, T. Miwa, T. Oono and S. Yamada, *Mater. Sci. Eng. B*, 2006, **132**, 74-78.

3   J. Lu and C. P. Wong, *IEEE Trans. Dielec. Elect. Insul.*, 2008, **15**, 1322-1328.

4   C. Pecharroman, F. E. Betegon, J. F. Bartolome, S. L. Esteban and J. S. Moya, *Adv. Mater.*, 2001, **13**, 1541-1544.

5   R. Koduri and M. Lopez, *Eur. Phys. J. Appl. Phys.*, 2007, **37**, 93-99.

6   J. Huang, Y. Cao and M. Hong, *Appl. Phys. Lett.*, 2008, **92**, 022911.

7   S. George and M. T. Sebastian, *J. Amer. Cer. Soc.*, 2007, **90**, 3522-3528.

8   S. George and M. T. Sebastian, *Compos. Sci. Technol.*, 2008, **68**, 2461-2467.

9   S. George, N. I. Santha and M. T. Sebastian, *J. Phys. Chem. Sol.*, 2009, **70**, 107-111.

10 P. H. Xiang, X. L. Dong, C. -D. Feng, R. -H. Liang and Y. -L. Wang, *Mater. Chem. Phys.*, 2006, **97**, 410-414.

11 P. S. Anjana, S. George and M. T. Sebastian, *J. Phys. D: Appl. Phys.*, 2009, **42**, 225502.

12   S. George and M. T. Sebastian, *Compos. Sci. Technol.*, 2009, **69**, 1298-1302.

13   H. Banno and K. Ogura, *Ferroelectrics*, 1989, **95**, 171-174.

14   Y. Daben, *Ferroelectrics*, 1990, **101**, 291-296.

15   Z. M. Dang, Y. H. Lin and C.W. Nan, *Adv. Mater.*, 2003, **15**, 1625-1629.

16   L. Qi, B. I. Lee, S. Chen, W. D. Samuels and G. J. Exarhos, *Adv. Mater.*, 2005, **17**, 1777-1781.

17   J. B. Ngoma, J. Y. Cavaille, J. Paletto, J. Perez and F. Macchi, *Ferroelectrics*, 1990, **109**, 205-210.

18   X. Jianwen, M. Kyoung-Sik, C. Tison and C. P. Wong, *IEEE Trans. Adv. Pack.*, 2006, **29**, 295-306.

19   S. George and M.T. Sebastian, *J. Appl. Polym. Sci.*, 2009, **114**, 1682-1686.

20   N. P. Bansal and Z. Zhong, *J. Power Sources*, 2006, **158**, 148-153.

21   E. Djurado and M. Labeau, *J. Eur. Ceram. Soc.*, 1998, **18**, 1397-1404.

22   R. Polini, A. Falsetti and E. Traversa, *J. Eur. Ceram. Soc.*, 2005, **25**, 2593-2598.

23   M. A. Senaris-Rodriguez and J. B. Goodenough, *J. Solid. State. Chem.*, 1995, **118**, 323-336.

24   A. N. Petrov, O. R. Kononchuk, A. V. Andreev, V. A. Cherepanov and P. Kofstad, *Solid State Ionics*, 1995, **80**, 189-199.

25   L. M. VanderHaar, M. W. D. Otter, M. Morskate, H. J. M. Bouwmeester and H. Verweij, *J. Electrochem. Soc.*, 2002, **149**, J41-J46.

26   H. Ohbayashi, T. Kudo and T. Gejo, *Jpn. J. Appl. Phys.*, 1974, **13**, 1-7.

27   A. Chainani, M. Mathew and D. D. Sarma, *Phys. Rev. B*, 1992, **46**, 9976-9983.

28   H. J. Kim, W. K. Choo and C. H. Lee, *J. Eur. Ceram. Soc.*, 2001, **12**, 1775-1778.

28

29 R. Dat, O. Auciello, D. J. Lichtenwalner and A. I. Kingon, *J. Mater. Res.*, 1996, **11**,1514-1519.

30 P. Kim, N. M. Doss, J. P. Tillotson, P. J. Hotchkiss, M. J. Pan, S. R. Marder, J. Li, J. P. Calame and J. W. Perry, *ACS Nano*, 2009, **3**, 2581-2592.

31 M. Arbatti, X. Shan and Z. Y. Cheng, *Adv. Mater.*, 2007, **19**, 1369-1372.

32 Z. M. Dang, L. Wang, H. Y. Wang, C. W. Nan, D. Xie, Y. Yin and S. Tjong, *Appl. Phys. Lett.*, 2005, **86**, 172905.

33 T. Zhou, J. W. Zha, R. Y. Cui, B. H. Fan, J. K. Yuan and Z. M. Dang, *ACS Appl. Mater. Interfaces*, 2011, **3**, 2184-2188.

34 L. Shaohui, Z. Jiwei, W. Jinwen, X. Shuangxi and Z. Wenquin, *ACS Appl. Mater. Interfaces*, 2014, **6**, 1533-1540.

35 S. H. Yao, Z. M. Dang, M. J. Jiang, H. P. Xu and J. Bai, *Appl. Phys. Lett.*, 2007, **91**, 212901.

36 M. Panda, V. Srinivas and A. Thakur, *Appl. Phys. Lett.*, 2008, **92**, 132905.

37 L. Wang and Z. M. Dang, *Appl. Phys. Lett.*, 2005, **87**, 042903.

38 J. K. Yuan, S. H. Yao, Z. M. Dang, A. Sylvestre, M. Genestoux and J. Bai, *J. Phys. Chem. C*, 2011, **115**, 5515-5521.

39 C. Xing, L. Zhao, J. You, W. Dong, X. Cao and Y. Li, *J. Phys. Chem. B*, 2012, **116**, 8312-8320.

40 N. P. Bansal and B. Wise, *NASA/TM*, 2011, 217222.

41 Y. Takahashi, Y. Matsubara and H. Tadokoro, *Macromolecules*, 1983, **16**, 1588-1592.

42 Y. Tadokoro and H. Tadokoro, *Macromolecules*, 1980, **13**, 1317-1318.

43   D. Naegele, D. Y. Yoon and M. G. Broadhurst, *Macromolecules*, 1978, **11**, 1297-1298.

44   G. Pfister, M. Abkowitz and R. G. Crystal, *J. Appl. Phys.*, 1973, **44**, 2064-2070.

45   V.V. Kochervinski, *Crystallog. Rep.*, 2003, **48**, 649-675.

46   K. Tashiro, K. Takano, M. Kobayashi, Y. Chatani and H. Tadokoro, *Polym. Bull.*, 1983, **10**, 464-469.

47   J.B. Lando and W.W. J. Doll, *J. Macromol. Sci., Part B: Phys.*, 1968, **2**, 205-208.

48   J. Datta and A. K. Nandi, *Polymer*, 1997, **38**, 2719-2724.

49   R. K. Layek, S. Samanta, D. P. Chatterjee and A. K. Nandi, *Polymer*, 2010, **51**, 5846-5856.

50   X. Huang, P. Jiang, C. Kim, F. Liu and Y. Yin, *Eur. Polym. J.*, 2009, **45**, 377-386.

51   J. Scheinbeim, C. Nakafuku, B. A. Newman and K. D. Pae, *J. Appl. Phys.*, 1979, **50** , 4399-4405.

52   T. Hattori, M. Hikosaka and H. Ohigashi, *Polymer*, 1996, **37**, 85-91.

53   W. A. Yee, M. Kotaki, Y. Liu and X.H. Lu, *Polymer*, 2007, **48**, 512-521.

54   R. Gregorio and M. Cestari, *J Polym Sci: Part B: Polym. Phys.*, 1994, **32**, 859-870.

55   S. B. Ince-Gundz, R. A. Alpern, D. Amarer, J. Crawford, B. Dolan, R. Kobylarz, M. Raveley and P. Cebe, *Polymer*, 2010, **51**, 1485-1493.

56   D. R. Dillion, K. K. Tenneti, C. Y. Li, F. K. Ko, I. Sics and B. S. Hsiao, *Polymer*, 2006, **47**, 1678-1688.

57   S. Manna and A. K. Nandi, *J. Phys. Chem. C*, 2007, **111**, 14670-14680.

58   A. K. Nandi and L. Mandelkern, *J. Polym. Sci., Part B: Polym. Phys.*, 1991, **29**, 1287-1297.

59   W. M. Prest Jr. and D. J. Luca, *J. Appl. Phys.*, 1975, **46**, 4136-4143.

60   J. S. Andrew and D. R. Clarke, *Langmuir*, 2008, **24**, 670-672.

61   V. Sencadas, P. Martins, A. Pitaes, M. Benelmekki, J. L. G. Ribelles and S. Lanceros-Mendez, *Langmuir*, 2011, **27**, 7241-7249.

62   V. Singh, A. R. Kulkarni and T. R. R. Mohan, *J. Appl. Polym. Sci.*, 2003, **90**, 3602-3608.

63   Z. M. Dang, T. Zhou, S. H. Yao, J. K. Yuan, J. W. Zha, H. T. Song, J. Y. Li, Q. Chen, W. T. Yang and J. Bai, *Adv. Mater.*, 2009, **21**, 2077-2082.

64   T. J. Lewis, *J. Phys. D Appl. Phys.*, 2005, **38,** 202.

65   F. Claro, *Phys. Rev. B*, 1982, **25,** 7875-7876.

66   V. Ambegaokar, B. I. Halperin and J. S. Langer, *Phys. Rev. B*, 1971, **4**, 2612-2620.

67   P. Sheng, B. Abeles and Y. Arie, *Phys. Rev. Lett.*, 1973, **31,** 44-47.

68   D. Toker, D. Azulay, N. Shimoni, I. Balberg and O. Millo, *Phys. Rev. B*, 2003, **68,** 041403.

69   F. Claro, *Phys. Rev. B*, 1984, **30**, 4989-4999.

70   K. S. Deepa, M. T. Sebastian and J. James, *Appl. Phys. Lett.*, 2007, **91**, 202904.

71   K. S. Deepa, S. K. Nisha, P. Parameswaran, M. T. Sebastian and J. James, *Appl. Phys. Lett.*, 2009, **94**, 142902.

72   M. G. Todd and F.G. Shi, *J. Appl. Phys.*, 2003, **94**, 4551-4558.

73   I. A. Tchmutin, A. T. Ponomarenko, V. G. Shevchenko, N. G. Ryvkina, C. Klason and D. H. Mcqueen, *J. Polym. Sci: Part B Polym. Phys.*, 1998, **36**, 1847-1856.

74   Y. Song, T. W. Noh, S. I. Lee and J. R. Gaines, *Phys. Rev.* B, 1986, **33**, 904-908.